DOI 10.1007/s10812-025-01845-w
Journal of Applied Spectroscopy, Vol. 91, No. 6, January, 2025 (Russian Original Vol. 91, No. 6, November–December, 2024)

OPTICAL AND ELECTRICAL PROPERTIES OF $Sb_2(S_xSe_{1-x})_3$ FILMS FOR SOLAR CELLS

M. S. Tivanov,[a,*] T. M. Razykov,[b,c] K. M. Kuchkarov,[b,c] L. S. Lyashenko,[a] E. S. Voropay,[a] Sh. B. Utamurodova,[c] D. Z. Isakov,[b] M. A. Makhmudov,[b] A. N. Olimov,[b] S. A. Muzafarova,[c] and D. S. Bayko[a]

UDC 538.97

The vacuum thermal evaporation method was used to produce $Sb_2(S_xSe_{1-x})_3$ films from powders of precursor binary compounds, Sb_2S_3 and Sb_2Se_3, at substrate temperature 300°C. The effect of the elemental composition ratio S/(S + Se) on the optical and electrical properties of $Sb_2(S_xSe_{1-x})_3$ films was studied. The band gap width of $Sb_2(S_xSe_{1-x})$ films increases with an increase in the sulfur concentration. The prepared films feature low Urbach energies indicating low-defect structure. The temperature dependence of the resistance indicated the presence of deep-lying levels in the range 0.5–0.8 eV depending of the S/(S+Se) atomic concentration ratio. These results indicate the feasibility of producing effective solar cells containing $Sb_2(S_xSb_{1-x})_3$ obtained by means of thermal evaporation of powders of Sb_2S_3 and Sb_2Se_3.

Keywords: *Sb_2Se_3, Sb_2S_3, $Sb_2(Se,S)_3$, absorption coefficient, band gap width, Urbach energy, and conductivity.*

Introduction. The growing worldwide demand for electrical energy has led to a search for reliable and accessible photoelectric materials. At present, polycrystalline silicon (Si), cadmium telluride (CdTe), copper selenide ($CuSe_2$), indium selenide ($InSe_2$), and gallium selenide ($GaSe_2$) (CIGS) are used as solar absorbers in solar cells (SC) and have certified power conversion efficiency (PCE) >20% [1, 2]. The high cost for the conversion of silica to silicon, the toxicity of cadmium, high prices of gallium and indium, as well as insufficient reserves of indium, gallium, and tellurium have hindered the mass production of thin-film SC using these elements [3]. In order to overcome environmental problems as well as difficulties related to insufficient material for mass production, a new solar cell based on Cu_2ZnSnS_4 (CZTS) has been proposed for the absorbing layer. This compound has a structure similar to $Cu(In,Ga)(Se,S)_2$ where indium and gallium are replaced by zinc and tin, which are more available on the Earth's surface. Efficiency of 12.6% has been achieved at an IBM research center for a SC based on $Cu_2ZnSnS_xSe_{4-x}$ [4], which is much less efficient than for cells with $Cu(In,Ga)(Se,S)_2$. This is attributed to difficulty in preparing and controlling the composition of $Cu_2ZnSnS_xSe_{4-x}$ [4].

At present, special interest is being given to the use of chalcogenides of binary compounds, Sb_2Se_3 and Sb_2S_3, and solid solutions $Sb_2(S_xSe_{1-x})_3$ as the absorbing layer of solar cells. The physical properties of these materials, which are *p*-type semiconductors (band gap width E_g = 1.1–1.8 eV, high absorption coefficient $\alpha > 10^5$ cm^{-1} in the visible region, low melting point 612°C for Sb_2Se_3 and 550°C for Sb_2Se_3 and high partial vapor pressure), are similar to the properties of $Cu(In,Ga)(Se,S)_2$ [5]. The chemical elements in these readily available materials are relatively inexpensive and resistant to external actions [6], which are prerequisites for the large-scale production of efficient SC.

The efficiency of thin-film SC derived from solid solutions $Sb_2(S_xSe_{1-x})_3$ is only 5.60–10.75% [7–10]. Similar to SC derived from CdTe and $Cu(In,Ga)(Se,S)_2$, these are very low values hindering common use. The efficiency can be raised by altering the band gap width of $Sb_2(S_xSe_{1-x})_3$ films. The theoretical maximum efficiency $Sb2(S_xSe_{1-x})_3$ SC is ~32.88% (the Shockley–Queisser limit) [11]. Since this maximum for solar cells has not yet been reached, there is hope that their efficiency can be raised. The limiting values of the no-load voltage (U_{XX}), the short circuit current (I_{SC}), and the flip-flop

*To whom correspondence should be addressed.

[a]Belarusian State University, Minsk, Belarus; email: tivanov@bsu.by; [b]Physicotechnical Institute of the Academy of Sciences of the Republic of Uzbekistan, Tashkent, Uzbekistan; [c]Institute of Semiconductor Physics and Microelectronics, Tashkent, Uzbekistan. Translated from Zhurnal Prikladnoi Spektroskopii, Vol. 91, No. 6, pp. 830–836, November–December, 2024. Original article submitted October 9, 2024.

(*FF*) for the SC with $Sb_2(S_xSe_{1-x})_3$ were calculated by Liu et al. [11]: U_{XX} = 1.122 V, I_{SC} = 32.88 mA, and *FF* ≤ 89.3%. According to Mustafa et al. [12], the parameters achieved for these SC are U_{XX} = 0.630 V, I_{SC} = 25.7 mA, and *FF* ≤ 67.85%. There has been only a slight improvement in the values for U_{XX} and *FF* in the past five years. A further increase in the efficiency of such solar cells can be achieved by raising U_{XX} and *FF*. According to various workers [13–15], the no-load voltage depends strongly on the method of obtaining the absorbing layer, the physical properties of the base layer, the structure of the solar cell, and the mechanism for current transfer to the $CdS/Sb_2(S_x,Se_{1-x})_3$ separation boundary of the solar cell [16–24].

In previous work [14, 15], we studied the structural and morphological properties of Sb_2Se_3 layers obtained by molecular-beam epitaxy (MBE) on powders of Sb_2Se_3 at different base temperatures. These films are enriched in antimony and have orthorhombic structure with predominant (120) and (221) orientations. The diameters of the crystal rods in the Sb_xSe_y films were 0.5–8 μm. The mean diameters and lengths of the Sb_xSe_y rods deposited with Sb/Se ratios 0.66 and 0.7 are almost identical (0.5–1 and 1–4 μm, respectively).

In the present work, we studied the optical and electrical properties of thin films of $Sb_2(S_xSe_{1-x})_3$ obtained by vacuum thermal evaporation onto glass plates, which can be used to create solar cells with planar glass/ITO/$CdS/Sb_2(S_xSe_{1-x})_3$/Au structure.

Experimental. Thin films of $Sb_2(S_xSe_{1-x})_3$ [x = S/(S + Se)] were obtained by vacuum thermal evaporation. The starting materials were Sb_2S_3 and Sb_2Se_3 powders of semiconductor purity (99.999%, from Hangzhou Kaiyada Semiconductor Materials Co., China) with different mass ratios $(Sb_2S_3/(Sb_2S_3 + Sb_2Se_3)$ = 0–1 ($m(Sb_2S_3)$ = 100–0 mg, $m(Sb_2Se_3)$ = 0–100 mg) (Table 1). The powders were evaporated using quartz evaporation crucibles. The distance between the base and the crucibles in the working chamber was 5 cm. A base made of soda–lime glass (SLG, 75 × 25 × 1.1-mm premium quality glass microscope slides, SUPER grade glass with polished edge, 90° angles, and matte field for marking) was used in the preparation of solar cells with structure ITO/$CdS/Sb_2(S_xSe_{1-x})_3$/ZnO/ZnO:Al/Au. The sample dimensions were 1.5 × 1.5 cm. Prior to deposition of the thin layers of $Sb_2(S_xSe_{1-x})_3$, the crucibles with the materials to be evaporated were degassed. The thin layers were deposited with residual pressure in the vacuum chamber 10^{-5}–10^{-6} mm Hg.

During the deposition of the $Sb_2(S_xSe_{1-x})_3$ films, the temperature of the substrate was 300°C. The temperature of the evaporator was maintained at constant ~600°C. The rate of deposition of the thin films was ~0.1 μm/min. After deposition, the films were slowly cooled at high vacuum. The thickness of the deposited films was found to be about 2 μm using a Saito FA 120 4C scale (with precision of 0.1 mg).

The chemical composition of the resultant films was determined by energy-dispersive x-ray (EDX) analysis using an Oxford Instruments Aztec Energy Advanced X-Max-80 spectrometer with 20 kV accelerating voltage and penetration depth ~1.6 μm. The chemical element composition in the samples is given in Table 1, which shows that all the films have stoichiometric or close-to-stoichiometric composition. The thicknesses of the resultant thin films of $Sb_2(S_xSe_{1-x})_3$ were determined more precisely from microphotographs of the cross sections of the prepared samples using a LEO1455VP scanning electron microscope. For the following S/(S + Se) ratios, we found d (in μm): 0, d = 3.5–4; 0.14, d = 2.5–3; 0.22, d = 3–3.5; 0.40, d = 3.5–4; 0.43, d = 2–2.5; 0.53, d = 2–3; 0.67, d = 2.8–3.5; 0.82, d = 2–2.5; 0.84, d = 3–3.5; and 1.00, d = 2.5–3.

We used 3 × 5-mm samples with silver paste contacts for the electrical measurements. The distance between the contacts was 0.4–0.7 mm. The *p*-type conductivity was determined judging from the sign of the thermal electromotive force (EMF). The temperature dependence of the resistance was found using a two-zone method with a high-temperature cell permitting measurement of the resistance in vacuum with residual pressure p = 5 Pa at 300–440 K. In order to measure the resistance of the sample, we used a Keithley-2400 direct current source measure unit instrument as the source, permitting current measurement in the range 10^{-11}–1 A and voltage in the range 10^{-6}–100 V with error not more than ±0.1%. A Lakeshore 332 temperature controller was used to regulate and control the temperature in the sample. We used a Pt-100M resistance thermometer attached near the sample to measure the temperature with error ±0.3°C. The reflectance and transmission spectra were taken with spectral resolution ≤5 nm in the wavelength region 400–3000 nm with unpolarized light using an Essent Optics Photon RT multifunctional scanning spectrometer. The dimensions of the optical radiation beam on the surface of the sample studied were ~2 × 5 mm.

Results and Discussion. The experimental dependence curves for the reflectance (R) and transmission coefficients (T) on the radiation wavelength (λ) in the range 400–3000 nm in unpolarized light are given in Fig. 1. The reflection spectra show periodic peaks and depressions due to interference, which indicates high structural perfection of these thin films. A close-to-zero transmission coefficient T is found in Fig. 1b for these films in the range 400–900 nm, which then

TABLE 1. Chemical Composition of the Thin Films of $Sb_2(S_xSe_{1-x})_3$

Sample No.	1	2	3	4	5	6	7	8	9	10
$m(Sb_2Se_3)$, mg	100	90	80	70	60	50	40	30	20	0
$m(Sb_2S_3)$, mg	0	10	20	30	40	50	60	70	80	100
[Sb], at.%	40.22	40.38	40.53	39.9	39.81	39.76	39.93	39.45	38.92	40.76
[S], at.%	–	8.29	12.98	23.87	25.67	32.73	40.09	49.75	51.26	59.24
[Se], at.%	59.78	51.33	46.49	36.23	34.51	27.51	19.98	10.8	9.83	–
Sb/(S + Se)	0.67	0.68	0.68	0.66	0.66	0.66	0.66	0.65	0.64	0.69
x = S/(S + Se)	0.00	0.14	0.22	0.40	0.43	0.53	0.67	0.82	0.84	1.00

increases with increasing wavelength. The optical absorption indices (a) of the $Sb_2(S_xSe_{1-x})_3$ films were calculated using the experimental transmission and reflection data:

$$\alpha = -\frac{1}{4}\ln\left(\frac{\sqrt{(1-R)^4 + 4T^2R^2} - (1-R)^2}{2TR^2}\right), \quad (1)$$

where t is the sample thickness, R is the reflection coefficient, and T is the transmission coefficient [25].

A region of fundamental absorption corresponding to band-to-band electron transitions can be discerned in the dependence of the absorption index on wavelength. Using the curve for $\alpha(h\nu)$ and assuming that direct band-to-band optical transitions are allowed, the optical band gap width E_g of the films was found using the Tauc equation:

$$(\alpha h\nu)^2 = A(h\nu - E_g), \quad (2)$$

where $h\nu$ is the energy of the incident photon and A is a constant.

The band gap width of the films studied E_g was determined by extrapolation of the linear segment of the curve for $(\alpha h\nu)^2$ as a function of $h\nu$ to the abscissa. Curves for the spectral dependence of $(\alpha h\nu)^2$ on $h\nu$ for the films of $Sb_2(S_xSe_{1-x})_3$ and the calculated band gap width are shown in Fig. 2. The values obtained for E_g of these films with different values of x = S/(S + Se) correspond to the results of Yang [26] and Jiménez [27]. An increase in the band gap width is observed from 1.09 eV for Sb_2Se_3 to 1.65 eV for Sb_2S_3 with increasing concentration of sulfur in the prepared thin films of $Sb_2(S_xSe_{1-x})_3$. The dependence of the band gap width E_g on the sulfur fraction in these films is shown in the insert in Fig. 2. The thin films of $Sb_2(S_xSe_{1-x})_3$ obtained with S/(S + Se) ratios 0.00, 0.14, 0.22, 0.40, 0.43, 0.53, and 0.67 have band gap widths corresponding to the interval of the most efficient photoelectric conversion 1.1–1.5 eV [7]. The possibility of varying the band gap width by altering the S/(S + Se) ratio permits us to prepare films of $Sb_2(S_xSe_{1-x})_3$ in efficient solar cells for use both with and without solar radiation concentrators. According to calculations based on the Shockley–Queisser theory [28], the optimal S/(S + Se) ratio for the case of total solar radiation concentration (the solid angle, at which the sun is visible, 4π sr) for a photoabsorbing layer of $Sb_2(S_xSe_{1-x})_3$ is 0–0.1 (E_g ~ 1.1 eV), while in the case of a normal concentration (AM0 and the solid angle, at which the sun is visible $6.65\cdot10^{-5}$ sr), the optimum S/(S+Se) ratio is 0.3–0.4 (E_g ~ 1.3 eV).

In the weak absorption segment, the curve for α as a function of $h\nu$ shows exponential growth. This segment (known as the Urbach tail [29]) is observed due to optical absorption on discrete levels in the band gap corresponding to defects in the crystal lattice. The extent of disorder of the crystal lattice can be evaluated relative to the Urbach energy E_U. The empirical Urbach rule is obeyed in the low photon energy region ($h\nu \le E_g$):

$$\alpha = \alpha_0 \exp(h\nu/E_U), \quad (3)$$

where α_0 is a constant.

The value of E_U can be found from the slope of the linear segment of the curve for ln α as a function of $h\nu$ (Fig. 3). The relationship of the Urbach energy to the sulfur fraction in the films is shown in the insert in Fig. 3. The Urbach energy

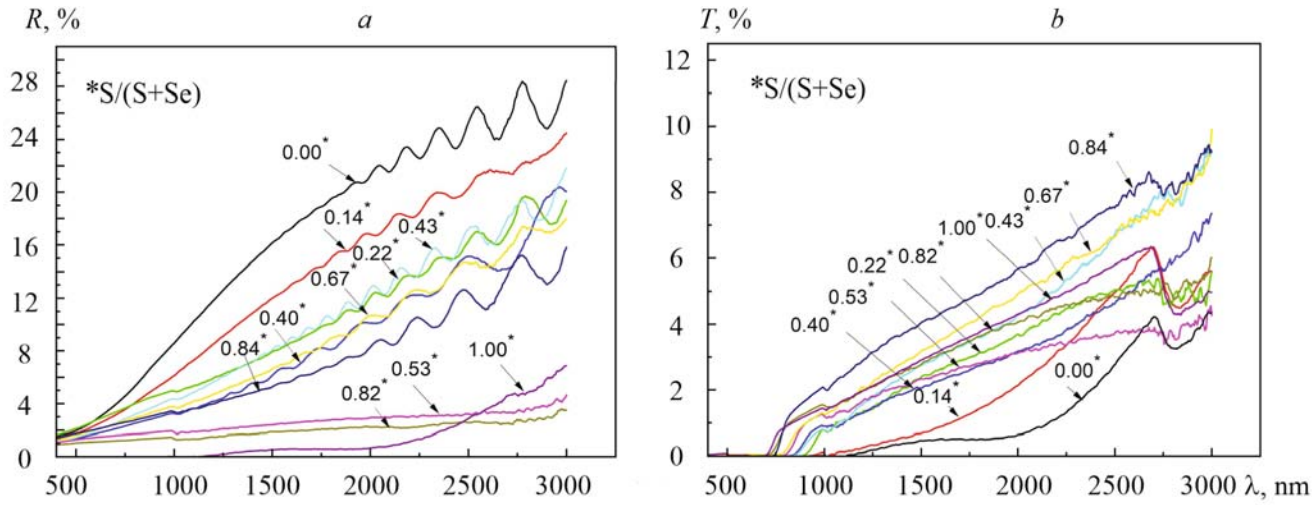

Fig. 1. Reflection $R(\lambda)$ (a) and transmission spectra $T(\lambda)$ (b) of thin films of $Sb_2(S_xSe_{1-x})_3$.

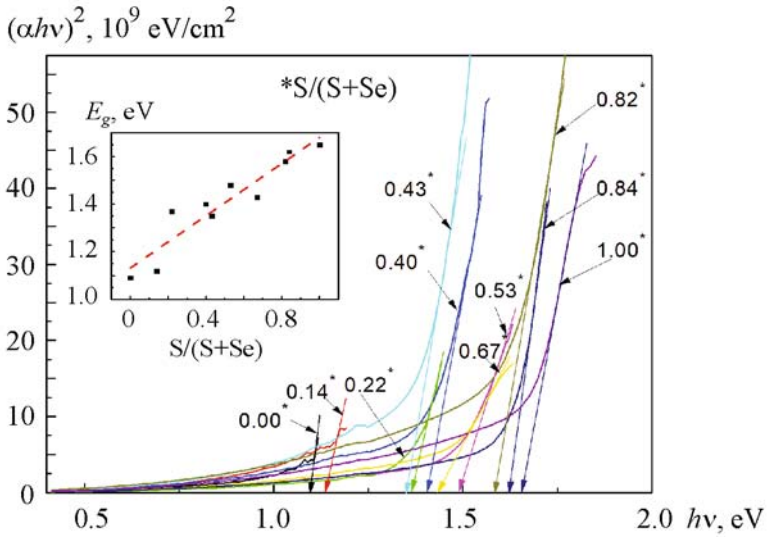

Fig. 2. Tauc plot used to determine the band gap width of thin films of $Sb_2(S_xSe_{1-x})_3$. The dependence of the band gap width E_g on the sulfur fraction in thin films of $Sb_2(S_xSe_{1-x})_3$ is given in the insert.

for all the samples was in the range 0.16–0.35 eV, which indicates rather low defectivity of these films. No dependence of E_U on the sulfur fraction was found.

Knowledge of the electrophysical parameters of the photoabsorbing layers is required for the creation of photoelectric converters. The shape of the temperature dependence of the specific electrical conductance in the Arrhenius plot shown in Fig. 4 for our thin films of $Sb_2(S_xSe_{1-x})_3$ suggests an activation mechanism for electron transfer with a constant activation energy E_a, which can be calculated using the following equation:

$$\sigma = s_0 \exp\left(-(E_a/kT)\right), \tag{4}$$

where σ is the specific electrical conductance, k is the Boltzmann constant, and T is the temperature. These values were used to construct curves for the dependence of the activation energy on the sulfur fraction in the thin films (insert in Fig. 4).

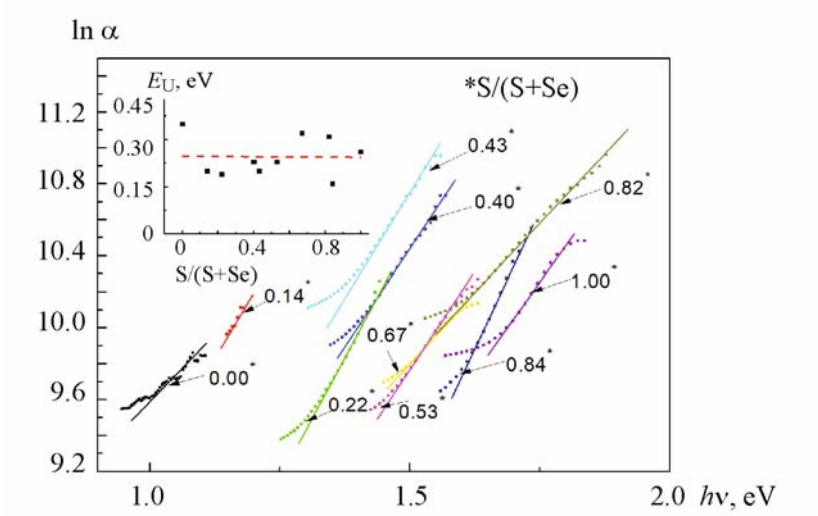

Fig. 3. Determination of the Urbach energy E_U of films of $Sb_2(S_xSe_{1-x})_3$. The dependence of the Urbach energy E_U on the sulfur fraction in films of $Sb_2(S_xSe_{1-x})_3$ is shown in the insert.

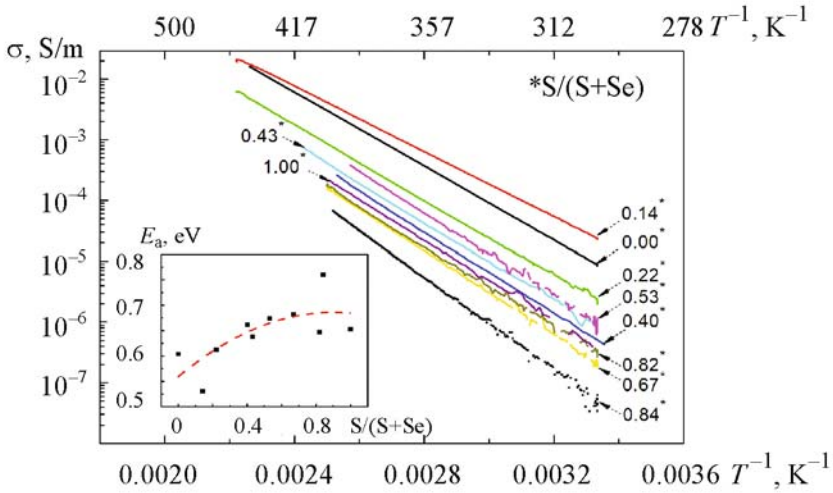

Fig. 4. Arrhenius plot for the temperature dependence of the specific electrical conductance of films of $Sb_2(S_xSe_{1-x})_3$. The insert gives the dependence of conductance of thin films of $Sb_2(S_xSe_{1-x})_3$ on the sulfur fraction.

According to Jiménez [27], the energy levels with the calculated depth are caused mainly by interaction of antimony 5*p* electrons with sulfur 3*p* electrons and/or selenium 4*p* electrons. With increasing sulfur fraction in the samples, the sulfur 3*d* electrons also begin to make a significant contribution to the density of states, which leads to a greater number of levels in the band gap and, as a consequence, a greater activation energy. A similar trend is observed in this work.

Conclusions. Optical reflection and transmission spectroscopy was used to determine the band gap width and Urbach energy of thin films of $Sb_2(S_xSe_{1-x})_3$ obtained by vacuum deposition with different sulfur/selenium ratios. The band gap width of these films for direct optical transitions ranges from ~1.1 to ~1.7 e/v with increasing S/(S + Se) ratios from 0 to 1. The Urbach energy is rather low (0.16–0.35 eV), which suggests low defectivity of these films. The temperature dependence of the electrical resistance was used to establish the existence of deep levels in the band gap of the thin films with electrical conductance activation energy increasing from ~0.6 to ~0.7 eV with increasing sulfur fraction. The

possibility of varying the band gap width in the region of maximum photoelectron conversion according to the Shockley–Queisser theory and the sufficiently sharp absorption edge according to the Urbach criterion indicate promise for the use of films of $Sb_2(S_xSe_{1-x})_3$ as components in efficient solar cells. For total solar radiation concentration, the optimal S/(S + Se) ratio for the photoabsorbing layer of $Sb_2(S_xSe_{1-x})_3$ is 0–0.1 (E_g ~ 1.1 eV) while the optimal ratio is 0.3–0.4 (E_g ~ 1.3 eV) for normal concentration.

Acknowledgments. This work was carried out with the support of the Ministry of Innovative Development of the Republic of Uzbekistan (Grant No. MRB-2021-540) and the State Committee on Science and Technology of the Republic of Belarus (Grant No. F21UZBG-022).

REFERENCES

1. M. A. Green, E. D. Dunlop, J. Hohl-Ebinger, M. Yoshita, N. Kopidakis, and X. Han, *Prog. Photovolt.: Res. Appl.*, **31**, 3–16 (2023); doi: 10.1002/pip.3646.
2. *Photovoltaics Report*, Fraunhofer Institute for Solar Energy Systems. ISE with Support of PSE Projects Gmbh [Online], https://www.ise.fraunhofer.de/content/dam/ise/de/documents/publications/studies/PhotovoltaicsReport.pdf [Accessed Nov. 12, 2023].
3. T. M. Razykov, C. S. Ferekides, D. Morel, E. Stefanakos, H. S. Ullal, and H. M. Upadhyaya, *Solar Energy*, **85**, 1580–1608 (2011); doi: 10.1016'j.solener.2010.12.002.
4. Y. Cao, C. Wang, B. Li, K. Zhang, X. Xu, J. Hu, and X. Chen, *Jpn. J. Appl. Phys.*, **50**, Article ID 125001 (2011); doi: 10.1143/JJAP.50.125001.
5. X. Wang, R. Tang, Ch. Wu, Ch. Zhu, and T. Chen, *J. Energy Chem.*, **27**, 713–721 (2018); doi:10.1016/j.jechem.2017.09.031.
6. A. Mavlonov, T. Razykov, R. Raziq, J. Gan, J. Chantana, Y. Kawano, T. Nishimura, H. Wei, A. Zakutayev, T. Minemoto, X. Zu, S. Li, and L. Qiao, *Solar Energy*, **201**, 227–246 (2020); doi: 10.1016/j.soener.2020.03.009.
7. Y. Zhou, L. Wang, S. Chen, S. Qin, X. Liu, J. Chen, D.-J. Xue, M. Luo, Y. Cao, Y. Cheng, and J. Tang, *Nature Photon.*, **9**, 409–415 (2015); doi: 10.1038/nphoton.2015.78.
8. B. Yang, S. Qin, D. Xue, L. Jiang, R. Tang, Ch. Jiang, Ch. Wu, D. Gao, X. Wang, F. Fang, Ch. Zhu, and T. Chen, *Prog. Photovolt.: Res. Appl.*, **25**¸ 113–122 (2017); doi: 10.1002/pip.2819.
9. X. Hu, J. Tao, R. Wang, Y. Pan, G. Weng, X. Luo, Sh. Chen, Z. Zhu, J. Chu, and H. Akiyama, *J. Power Sources*, **493**, Article ID 229737 (2021); doi: 10.1016/jpowsour.2021.229737.
10. X. Wang, R. Tang, Ch. Jiang, W. Lian, H. Ju, G. Jiang, Zh. Li, Ch. Zhu, and T. Chen, *Adv. Energy Mater.*, Article ID 2002341 (2020); doi: 10.1002/aenm.202002341.
11. X. Liu, Z. Xiao, Y. Yang, D. J. Xue, D. B. Li, Ch. Chen, Sh. Lu, L. Gan, Y. He, and M. C. Beard, *Prog. Photovolt.: Res. Appl.*, **25**, No. 10, 861–870 (2017).
12. F. I. Mustafa, S. Gupta, N. Goyal, and S. K. Tripathi, *J. Optoelectron. Adv. Mater.*, **11**, No. 12, 2019–2023 (2021).
13. Y. Mamta, Y. Singh, K. K. Maurya, and V. N. Singh, *Solar Energy Mater. Solar Cells*, **230**, Article ID 111223 (2021); doi: 10.1016/j.solmat.2021.111223.
14. T. M. Razykov, A. Kh. Shukurov, K. M. Kuchkarov, V. A. Ergashev, R. R. Khurramov, J. G. Bekmirzoyev, and A. A. Mavlonov, *Appl. Solar Energ.*, **55**, 376–379 (2019); doi: 10.3102/S0003701X19060094.
15. T. M. Razykov, K. M. Kuchkarov, M. S. Tivanov, V. A. Ergashev, R. Khurramov, D. Z. Isakov, A. Olimov, D. S. Baiko, N. I. Polyak, O. V. Korolik, and S. D. Sharipov, *Appl. Solar Energy*, **58**, No. 4, 461–465 (2022); doi: 10.3103/S0003801X22040132.
16. G.-X. Liang, X.-H. Zhang, H.-L. Ma, J.-G. Hu, B. Fan, Zh.-K. Luo, Zh. H. Zheng, J. T. Luo, and P. Fan, *Solar Energy Mater. Solar Cells*, **160**, 257–262 (2017); doi: 10.1016/j.solmat.2016.10.042.
17. O. S. Hutter, L. J. Phillips, P. J. Yates, J. D. Major, and K. Durose, *IEEE 7th World Conf. on Photovoltaic Energy Conversion (WCPEC)*, 0027–0031 (2018); doi: 10.1109/PVSC.2018.8547653.
18. X. Liu, J. Chen, and M. Luo, *Appl. Mater. Interfaces*, **6**, 10687–10695 (2014); doi: 10.1021/am502427s.
19. Y. H. Kwon, Y. B. Kim, M. Jeong, H. W. Do, H. K. Cho, and J. Y. Lee, *Solar Energy Mater. Solar Cells*, **172**, 11–17 (2017); doi: 10.1016;j.solmat.2017.07.004.
20. H. M. Pathan and Ch. D. Lokhande, *Bull. Mater. Sci.*, **27**, No. 2, 85–111 (2004); doi: 10.1007/BF02708491.
21. A. Kulkarni, S. Arote, H. Pathan, and R. S. Patil, *Mater. Renew. Sustain. Energy*, **4**, No. 1 (2015); doi: 10.1007/s40243-015-0058-5.

22. Y. Zhou, M. Leng, Z. Xia, J. Zhong, H. Song, X. Liu, B. Yang, Ju. Zhang, J. Chen, K. Zhou, J. Han, Y. Cheng, and J. Tang, *Adv. Energy Mater.*, **4**, Article ID 1301846 (2014); doi: 10.1002/aenm.201301846.
23. M. D. Khan, M. Aamir, M. Sohail, M. Sher, J. Akhtar, M. A. Malik, and N. Revaprasadu, *Solar Energy*, **169**, 526 (2018); doi: 10.1016/j.solener.2018.05.026.
24. L. Wang, D.-B. Li, K. Li, C. Chen, Ch. Chen, H. X. Deng, L. Gao, Y. Zhao, F. Jiang, L. Li, Fe. Huang, Y. He, H. Song, G. Niu, and J. Tang, *Nature Energy*, **2**, No. 4, 17046 (2017); doi: 10.1038/nenergy.2017.46.
25. D. K.Schroder, *Semiconductor Material and Device Characterization*, John Wiley & Sons, New York (1990).
26. B. Yang, D.-J. Xue, M. Leng, J. Zhong, L. Wang, H. Song, Y. Zhou, and J. Tang, *Sci. Rep.*, Article ID 10978 (2015); doi: 10.1038/srep10978(2015).
27. T. Jiménez, C. I. León-Pimentel, Di Seuret-Jiménez, and M. Courel, *General Chem.*, **5**, No. 2, Article ID 180029 (2019); doi: 10.21127/yaoyige20180029.
28. M. Tivanov, A. Moskalev, I. Kaputskaya, and P. Zhukowski, *Przegląd Elektrotechniczny*, **92**, No. 8, 85–87 (2016); doi: 10.15199/48.2016.08.23.
29. P. Urbach, *Phys. Rev. J.*, **92**, 1324 (1953); doi: 10.1103/PhysRev.92.1324.